Differential interactions of the formins INF2, mDia1, and mDia2 with microtubules

Jeremie Gaillard[a], Vinay Ramabhadran[b], Emmanuelle Neumanne[c], Pinar Gurel[b], Laurent Blanchoin[a], Marylin Vantard[a], and Henry N. Higgs[b]

[a]CEA, iRTSV, Laboratoire Physiologie Cellulaire & Végétale, CNRS, UMR5168, Université Joseph Fourier-Grenoble I, F-38054 Grenoble, France; [b]Department of Biochemistry, Dartmouth Medical School, Hanover, NH 03755; [c]Institut de Biologie Structurale Jean-Pierre Ebel, CNRS, CEA, University Joseph Fourier, F-38027 Grenoble, France

ABSTRACT **A number of cellular processes use both microtubules and actin filaments, but the molecular machinery linking these two cytoskeletal elements remains to be elucidated in detail. Formins are actin-binding proteins that have multiple effects on actin dynamics, and one formin, mDia2, has been shown to bind and stabilize microtubules through its formin homology 2 (FH2) domain. Here we show that three formins, INF2, mDia1, and mDia2, display important differences in their interactions with microtubules and actin. Constructs containing FH1, FH2, and C-terminal domains of all three formins bind microtubules with high affinity (K_d < 100 nM). However, only mDia2 binds microtubules at 1:1 stoichiometry, with INF2 and mDia1 showing saturating binding at approximately 1:3 (formin dimer:tubulin dimer). INF2-FH1FH2C is a potent microtubule-bundling protein, an effect that results in a large reduction in catastrophe rate. In contrast, neither mDia1 nor mDia2 is a potent microtubule bundler. The C-termini of mDia2 and INF2 have different functions in microtubule interaction, with mDia2's C-terminus required for high-affinity binding and INF2's C-terminus required for bundling. mDia2's C-terminus directly binds microtubules with submicromolar affinity. These formins also differ in their abilities to bind actin and microtubules simultaneously. Microtubules strongly inhibit actin polymerization by mDia2, whereas they moderately inhibit mDia1 and have no effect on INF2. Conversely, actin monomers inhibit microtubule binding/bundling by INF2 but do not affect mDia1 or mDia2. These differences in interactions with microtubules and actin suggest differential function in cellular processes requiring both cytoskeletal elements.**

Monitoring Editor
Thomas D. Pollard
Yale University

Received: Jul 12, 2011
Revised: Sep 7, 2011
Accepted: Sep 30, 2011

INTRODUCTION

Actin filaments and microtubules play coordinated roles in a wide variety of cellular processes, including cell migration, membrane transport, and cell division (reviewed in Goode *et al.*, 2000; Rodriguez *et al.*, 2003). In addition, there is evidence that these two cytoskeletal elements interact physically in cytoplasm (Schliwa and van Blerkom, 1981; Waterman-Storer *et al.*, 2000; Schuh and Ellenberg, 2008; Korobova and Svitkina, 2010). The proteins that link actin and microtubules in specific processes are still largely a matter of debate. A number of proteins could serve as intermediaries by binding both actin filaments and microtubules, including formins (reviewed in Bartolini and Gundersen, 2010), adenomatous polyposis coli (APC; Okada *et al.*, 2010), myosin 1C (Rump *et al.*, 2011), and doublecortin (Tsukada *et al.*, 2005). Other proteins, such as WHAMM, WASH, and JMY, could serve as links by binding Arp2/3 complex and microtubules (reviewed in Rottner *et al.*, 2010).

The large number of mammalian formin proteins (15 genes and multiple splice variants; Higgs and Peterson, 2005) provides

This article was published online ahead of print in MBoC in Press (http://www.molbiolcell.org/cgi/doi/10.1091/mbc.E11-07-0616) on October 12, 2011.

Address correspondence to: Henry Higgs (henry.n.higgs@dartmouth.edu), Marylin Vantard (marylin.vantard@cea.fr).

Abbreviations used: DAD, diaphanous autoregulatory domain; FH1FH2C, protein construct containing the FH1, FH2, and C-terminal domains; FH2, formin homology 2 domain; GST, glutathione *S*-transferase; LatB, Latrunculin B; MT, microtubule; TIRF, total internal reflection; WH2, WASP homology 2 domain.

wide-ranging possibilities for coordinating actin and microtubules. Formins bind actin mainly through their dimeric formin homology 2 (FH2) domain, which can both accelerate filament nucleation and modulate elongation rate by remaining bound to the growing filament barbed end (reviewed in Higgs, 2005). The FH1 domain, adjacent to the FH2, is proline rich and binds the actin monomer-binding protein profilin (reviewed in Paul and Pollard, 2009). Together, the FH1-FH2 domains accelerate elongation, with the FH2 domain bound to a filament barbed end and the profilin/actin–bound FH1 domain feeding actin monomers onto this barbed end. The C-terminal regions of some formins, including INF2 (Chhabra and Higgs, 2006), mDia1 (Gould *et al.*, 2011), and FMNL3 (Vaillant *et al.*, 2008; E. G. Heimsath and H. N. Higgs, unpublished results), also have actin binding ability and contribute to actin dynamics.

Formins vary in their effects on actin. Whereas mDia1 appears to be confined to accelerating nucleation and barbed-end elongation, other formins have additional effects by virtue of actin filament side binding. Several formins bundle filaments, including Bnr1p, mDia2, Cappuccino, FMNL1, FMNL2, and FMNL3 (Moseley and Goode, 2005; Harris *et al.*, 2006, 2010; Quinlan *et al.*, 2007; Vaillant *et al.*, 2008). One formin, INF2, has the unique property of accelerating both filament polymerization and depolymerization, the depolymerization activity requiring an actin monomer–binding DAD/WH2 motif C-terminal to the FH2 (Chhabra and Higgs, 2006).

The microtubule-binding properties of formins have been less well characterized, but four mammalian formins (mDia2, INF1, formin1, and formin2) and one *Drosophila* formin (Cappuccino) have been shown to bind microtubules directly (Rosales-Nieves *et al.*, 2006; Zhou *et al.*, 2006; Quinlan *et al.*, 2007; Bartolini *et al.*, 2008; Young *et al.*, 2008). Of these formins, three (mDia2, formin2, and Cappuccino) require the FH2 domain for microtubule binding, and two (INF1 and formin1) use sequences outside the FH2. INF1 possesses two C-terminal microtubule-binding motifs capable of bundling microtubules in vitro and in cells (Young *et al.*, 2008), whereas regions in the N-terminus of formin2 appear to mediate microtubule binding (Zhou *et al.*, 2006). mDia2 constructs containing FH1, FH2, and C-terminal regions (FH1FH2C) stabilize microtubules against cold- and dilution-induced depolymerization (Bartolini *et al.*, 2008). Of interest, FH2 mutations that prevent actin association in mDia2 do not affect microtubule binding and stabilization (Bartolini *et al.*, 2008). Only one formin (Cappuccino) has been shown to bind actin filaments and microtubules simultaneously (Rosales-Nieves *et al.*, 2006). Microtubule binding by both formin2 and Cappuccino is inhibited by the Spire KIND domain (Quinlan *et al.*, 2007).

In cells, several formins have clear effects on microtubules. Overexpression of FH2-containing constructs for mDia1 (Ishizaki *et al.*, 2001) or FHOD1 (Gasteier *et al.*, 2005) causes alignment of actin filaments and microtubules. Expression or activation of either mDia1 or mDia2 causes an increase in stable microtubules, and mDia1 knockdown decreases stable microtubules in multiple cell types (reviewed in Bartolini and Gundersen, 2010). In addition to their own microtubule-binding ability, mDia1 and mDia2 can bind two other microtubule-binding proteins, APC and EB1 (Wen *et al.*, 2004). Another Dia formin, mDia3, is necessary for stable kinetochore–microtubule interaction (Yasuda *et al.*, 2004; Cheng *et al.*, 2011). Overexpression of INF1 C-terminus causes microtubule bundling and an increase in microtubule acetylation (Young *et al.*, 2008). Finally, there are several examples of formin-mediated microtubule network reorganization. During T cell–APC interaction, both mDia1 and FMNL1 are necessary for MTOC reorientation in T cells toward the antigen-presenting cell (Eisenmann *et al.*, 2007; Gomez *et al.*, 2007). During meiosis in mammalian oocytes, the spindle migrates to the cell periphery, dependent upon an actin meshwork assembled by formin2 (Azoury *et al.*, 2008; Li *et al.*, 2008; Schuh and Ellenberg, 2008). During *Drosophila* oocyte development, mutations in Cappuccino cause premature onset of microtubule-based cytoplasmic streaming (Theurkauf, 1994; Dahlgaard *et al.*, 2007).

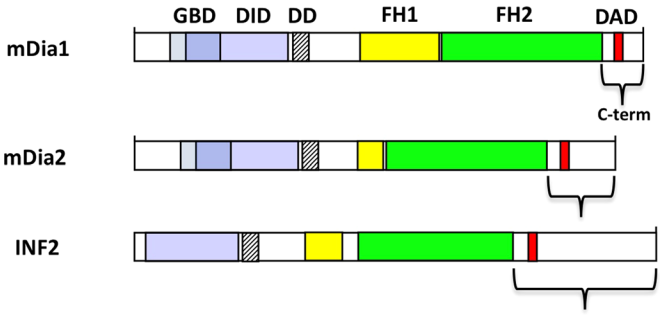

FIGURE 1: Schematic diagrams of mDia1, mDia2, and INF2 primary structures. Domain boundaries are approximately to scale. For the domains relevant to this work, the boundaries are as follows: mDia1 (mouse): 1255 residues total; FH1, 559–747; FH2, 752–1148; DAD, 1182–1192. mDia2 (mouse): 1171 residues total; FH1, 554–596; FH2, 615–1007; DAD, 1041–1051. INF2 (human, CAAX splice variant): 1249 residues total; FH1, 421–520; FH2, 554–940; DAD/WH2, 973–985. The C-terminal regions of the proteins are indicated by brackets: mDia1, 1149–1255; mDia2, 1009–1171; INF2, 941–1249. Boundaries of the constructs used for these studies are given in *Materials and Methods*.

To summarize, all formins tested are capable of binding microtubules, and formins can exert effects on microtubule stability and positioning in cells. In this study, we compare three formins, INF2, mDia1, and mDia2, to address fundamental features of microtubule binding and the crossover effects between actin and microtubules. We find that these formins display multiple differences in their interactions with microtubules, suggesting that formins differ in their abilities to interact simultaneously with actin filaments and microtubules in cells.

RESULTS

We compared the microtubule-binding properties of three formins, INF2, mDia1, and mDia2, focusing on the following aspects: microtubule-binding affinity and stoichiometry; microtubule-bundling activity; effects of microtubules on actin polymerization/depolymerization; and effect of actin on microtubule binding/bundling. The constructs used for these studies consist of the FH1 domains, FH2 domains, and C-terminal regions of these proteins (Figure 1), since these encompass the actin-binding regions and were used previously for microtubule-binding studies of mDia2 (Bartolini *et al.*, 2008).

Microtubule binding by INF2, mDia2, and mDia1 constructs

We used pelleting assays of Taxol-stabilized microtubules to determine binding affinity and stoichiometry for the FH1-FH2-C constructs of INF2, mDia1, and mDia2. All three formins bind microtubules with similar affinities of <100 nM (Figure 2A). However, there are substantial differences in binding stoichiometries, with mDia2 binding at ~1:1 (tubulin dimer:formin dimer) and INF2 and mDia1 binding at closer to 3:1 (Figure 2, A and E).

To test whether the C-terminal region contributes to microtubule-binding affinity or stoichiometry, we tested the FH1-FH2

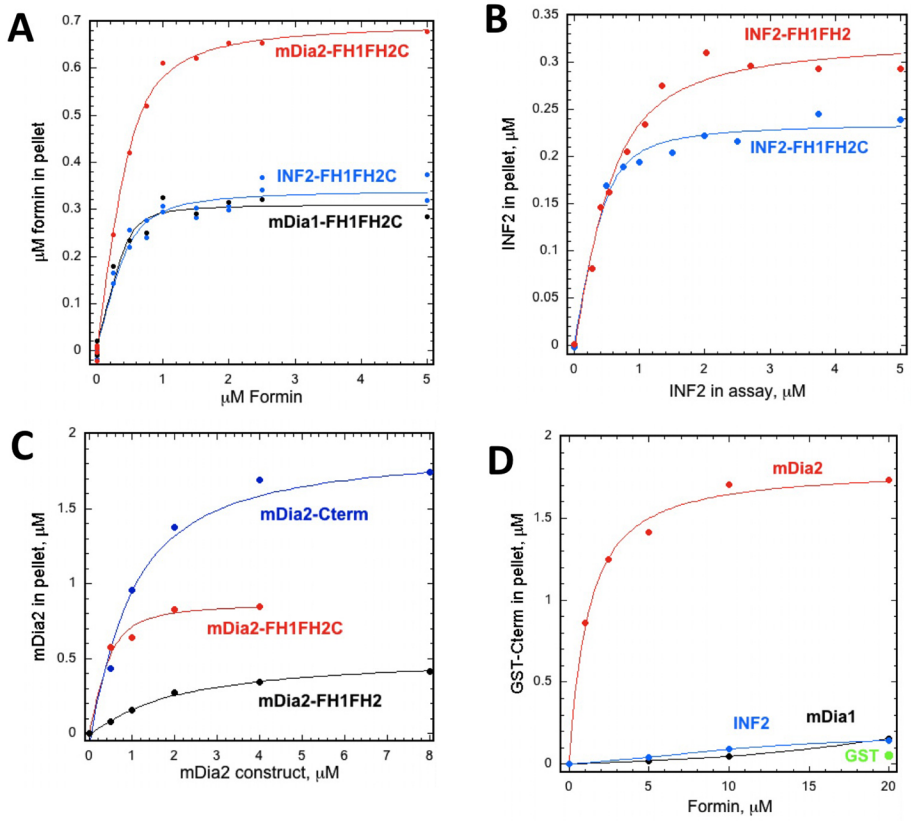

E **Stoichiometry at Saturation**

Formin	Tubulin:Formin
INF2-FH1FH2C	3.4:1
INF2-FH1FH2	2.7:1
mDia1-FH1FH2C	3.1:1
mDia2-FH1FH2C	0.9:1
mDia2-FH1FH2	1.7:1
mDia2-Cterm	0.6:1

FIGURE 2: Microtubule binding by constructs of INF2, mDia1, and mDia2. Pelleting assays using 0.5 μM polymerized tubulin (dimer), Taxol stabilized. Formin concentrations represent monomer concentration. (A) FH1FH2C constructs: INF2, mDia1, and mDia2. (B) INF2 constructs: FH1FH2C and FH1FH2. (C) mDia2 constructs: FH1FH2C, FH1FH2, and GST-Cterm. (D) GST fusions of C-termini of INF2, mDia1, and mDia2. Representative Coomassie-stained SDS–PAGE gels of some of the data are shown in Supplemental Figure S1. (E) Stoichiometries of formin binding to microtubules at saturation, determined by densitometry vs. a standard curve for each protein. Stoichiometries reflect the dimers of both tubulins and formins.

constructs of INF2 and mDia2 in microtubule pelleting assays. INF2-FH1FH2 binds microtubules with slightly lower affinity than the FH1-FH2-C construct (K_d of 250 vs. 90 nM) but with similar stoichiometry (2.6:1 vs. 3.4:1, tubulin dimer:formin dimer; Figure 2B). In contrast, the mDia2-FH1FH2 construct binds microtubules with considerably lower affinity (K_d of 1.8 μM vs. 65 nM) and lower stoichiometry (1.7:1 tubulin dimer:formin dimer; Figure 2C).

To test microtubule binding by the C-termini directly, we used glutathione *S*-transferase (GST)–fusion proteins of INF2, mDia1, and mDia2 constructs in microtubule pelleting assays. We consider the dimeric GST-fusion constructs to be more representative than the cleaved C-terminal constructs in these assays, since the C-terminus is normally adjacent to the dimeric FH2 domain. Furthermore, the fact that the C-termini are oriented in opposite directions in the GST dimer (McTigue *et al.*, 1995) bears some resemblance to the antiparallel orientation of the C-termini in the FH2 dimer (Xu *et al.* 2005). GST alone displays no apparent binding to microtubules when tested at 20 μM (Figure 2D).

The C-terminus of mDia2 binds microtubules with measurable affinity (K_d = 0.71 μM; Figure 2D). In addition, GST-mDia2-Cterm binds microtubules with higher stoichiometry (0.6:1 tubulin dimer:GST dimer) than the FH1FH2 or FH1FH2C constructs (Figure 2C). In contrast, the C-termini of INF2 and mDia1 display very low affinity for microtubules, with minimal binding at concentrations up to 20 μM (Figure 2D). To summarize, the C-terminus of mDia2 contributes appreciably to both microtubule-binding affinity and stoichiometry, whereas the C-termini of INF2 and mDia1 do not. Representative SDS–PAGE gels from the binding assays are shown in Supplemental Figure 1.

Microtubule bundling by formin constructs

Because both INF1 and mDia2 have been shown to bundle microtubules, we compared the bundling abilities of formin FH1-FH2-C constructs. In fluorescence microscopy assays using Taxol-stabilized microtubules (Alexa 568 labeled), INF2-FH1FH2C is a potent microtubule bundler. At a ratio of 4:1 tubulin:INF2 (dimer:dimer), the bundles are much longer than individual microtubules in the assay and incorporate INF2-FH1FH2C (fluorescein labeled) evenly along their length (Figure 3A), suggesting that INF2-FH1FH2C causes organization of bundles containing overlapping microtubules of varying length. Bundling can be detected at ratios as high as 10:1 tubulin:INF2 (unpublished data). In contrast, bundles are undetectable in assays containing equivalent amounts of INF2-FH1FH2 (Figure 3A). Similarly, mDia1-FH1FH2C does not cause noticeable microtubule bundling by this assay (Figure 3B). Small bundles of microtubules are evident in the presence of mDia2-FH1FH2C (Figure 3B), which is consistent with results for mDia2-FH1FH2 (Bartolini *et al.*, 2008). However, these bundles are not as extensive as those created by INF2-FH1FH2C. We also conducted assays in a Taxol-free system that allows microtubule dynamics. Under these conditions, INF2-FH1FH2C also assembles extensive microtubule bundles (Figure 3C).

We examined the INF2-FH1FH2C–induced bundles in greater detail using negative-stained electron microscopy. At a ratio of 1:1 (dimer:dimer), INF2-FH1FH2C causes assembly of thick bundles, often with widths of 100–125 nm (Figure 4). The majority of the bundles contain a large number of microtubules, and the overlapping nature of the microtubules complicates assessment of their detailed structure. Nevertheless, in the occasional bundles containing only a

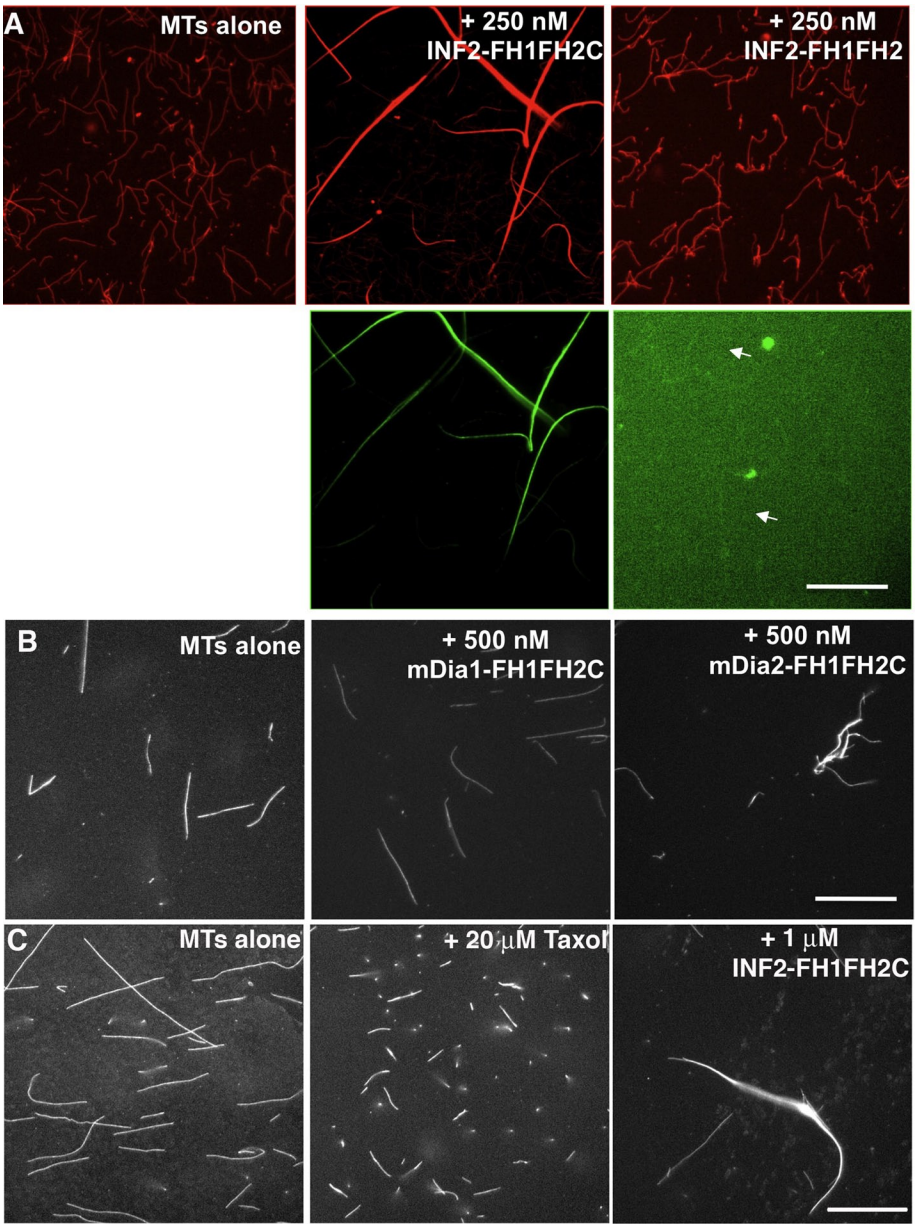

FIGURE 3: Fluorescence micrographs of microtubule bundling by INF2-FH1FH2C. (A) Fluorescence microscopy of Taxol-stabilized, Alexa 568–labeled microtubules (0.5 μM tubulin) in the absence or presence of fluorescein-labeled INF2-FH1FH2C or INF2-FH1FH2. Assays conducted in actin polymerization buffer. Arrows point to INF2-FH1FH2 labeling individual microtubules. (B) Fluorescence microscopy of Taxol-stabilized, Alexa 568–labeled microtubules in the absence or presence of 500 nM mDia1 or mDia2-FH1FH2C. Assays conducted in actin polymerization buffer. (C) Fluorescence micrographs of Alexa 568–tubulin (25 μM) polymerized in microtubule polymerization buffer for 45 min in the presence of the indicated additives. Formin monomer concentrations are given in all cases. Scale bars, 20 μm.

few microtubules, the intermicrotubule distance is 10–12 nm (Supplemental Figure 2A). This distance is significantly smaller than those we previously measured for two other bundling proteins: 30 nm for MAP65-1 (Gaillard *et al.*, 2008) and 15 nm for MAP65-4 (Fache *et al.*, 2010). In contrast to INF2-FH1FH2C, no clear microtubule bundles are detected in the presence of INF2-FH1FH2 (Figure 4), mDia1-FH1FH2C, or mDia2-FH1FH2C (Supplemental Figure 2B) using electron microscopy.

These microtubule-bundling results are supported by low-speed centrifugation assays, in which microtubule bundles sediment more readily than single microtubules (Gaillard *et al.*, 2008). INF2-FH1FH2C causes a significant shift of tubulin to the pellet fraction, whereas the INF2-FH1FH2 construct does not (Supplemental Figure 3A). For mDia2-FH1FH2C, there is a slight shift of tubulin to the pellet at higher concentrations, whereas mDia1-FH1FH2C does not have this effect (Supplemental Figure 3B). We note that bundling by INF2-FH1FH2C or mDia2-FH1FH2C is not due to aggregation of the formins prior to mixing with microtubules, since both formins have been shown to be dimeric by analytical ultracentrifugation (Li and Higgs, 2005; Chhabra and Higgs, 2006) and since the proteins are centrifuged at 100,000 × *g* for 15 min in binding buffer immediately prior to mixing with microtubules.

To examine the dynamics of INF2-mediated microtubule bundles, we used total internal reflection fluorescence (TIRF) microscopy of Alexa 568–labeled tubulin (red) in the presence of green fluorescent protein (GFP)–tagged INF2-FH1FH2C (green). In these experiments, we incubated GMPCPP-stabilized microtubules alone or preincubated with INF2 in order to obtain stable microtubule seeds that were further elongated by the addition of Alexa 568–tubulin with or without GFP-INF2 (Figure 5, A–C, and Supplemental Movies S1 and S2), as described for other microtubule-bundling proteins (Fache *et al.*, 2010). Microtubules elongate from both ends of the bundles, suggesting that individual microtubules in the bundle are in an antiparallel or random orientation (Supplemental Movie S1). Analysis of individual microtubule dynamics in these bundles is challenging due to the presence of multiple microtubules in close proximity. In particular, there is uncertainty as to whether the dynamics observed represents individual microtubules or two or more microtubules displaying similar dynamics. Nevertheless, we observe a number of interesting features. First, the frequency of clear catastrophe events is considerably decreased in bundles compared with individual microtubules. From analysis of 11 bundles for an average of 15 min per bundle, we identified only two clear catastrophe events (Figure 5C, stars) compared with the frequent catastrophes that occur in individual microtubules (Figure 5A, kymograph, stars). Second, there are occasional pauses in growth of the bundles (Figure 5C, blue lines). Between these pauses, there are sustained periods of growth of one or more microtubules in the bundle (Figure 5C, arrows), and the elongation rate in these periods is 1.5 μm/min (Figure 5D, n = 48), similar to the rate of microtubules that are not in bundles (1.7 μm/min (Figure 5A; Fache *et al.*, 2010). Third, the overall elongation rate of the bundles is slower (0.89 μm/min [n = 11]; Figure 5D) than the

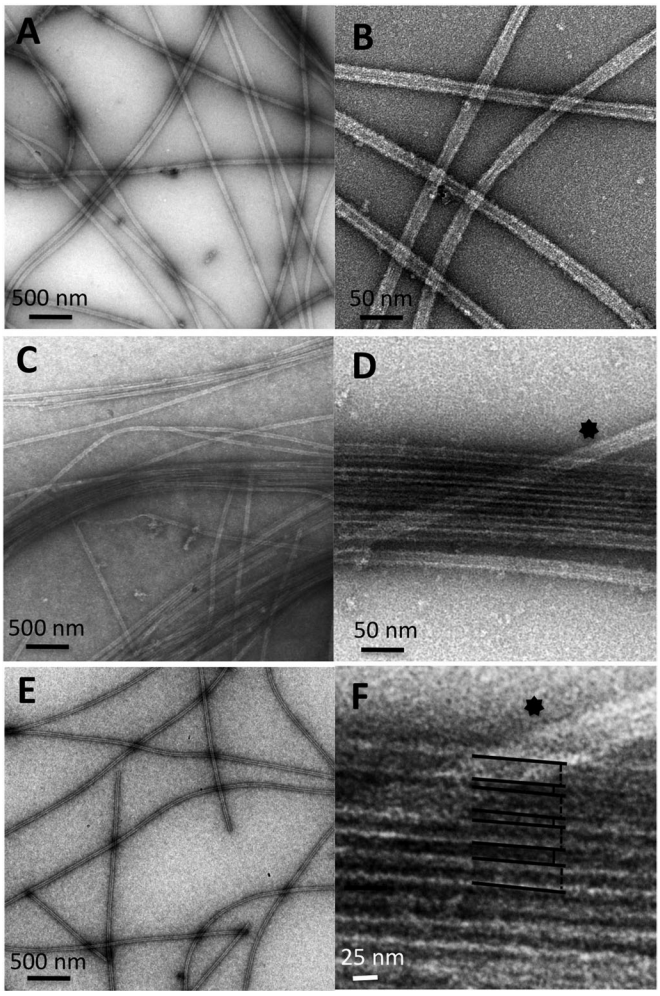

FIGURE 4: Negative-stained electron microscopy of microtubule bundles assembled by INF2-FH1FH2C. Taxol-stabilized microtubules (2 μM tubulin dimer) were incubated in the absence (E) or in the presence of 4 μM INF2-FH1FH2 (A, B) or 4 μM INF2-FH1FH2C (C, D, F). INF2 monomer concentrations are given. (F) High-magnification view of the MT bundle shown in D.

elongation rate of microtubules, suggesting that pauses must be more frequent than we observe, due to the complexity of the kymographs. Of interest, INF2 binding to growing microtubule bundles is rapid, as we observe no apparent region in which the red label precedes green on the elongating filament in the time-lapse acquisition of the experiment (one frame every 5 s; Figure 5B and Supplemental Movie S2).

Effects of microtubules on actin dynamics by INF2, mDia1, and mDia2

Because these formins can interact with both actin and microtubules, we asked whether the binding of one cytoskeletal component could affect binding of the other. We used pyrene–actin polymerization assays to test the effect of microtubules on the abilities of FH1FH2C constructs to accelerate actin polymerization. Before describing the results, we note that other buffer components introduced with the microtubules (Taxol, GTP, 1,4-piperazinediethanesulfonic acid [PIPES] buffer) are kept constant in the assays and do not affect the activities of the INF2, mDia1, and mDia2 constructs tested.

A concentration of microtubules (1.5 μM) sufficient to bind >95% of INF2-FH1FH2C has no apparent effect on its ability to accelerate actin polymerization (Figure 6A). In contrast, microtubules have a potent inhibitory effect on mDia2 in these assays, with concentrations as low as 30 nM suppressing actin polymerization significantly (Figure 6B). In addition, mDia2's C-terminus is required for inhibition by microtubules, since actin polymerization by mDia2-FH1FH2 is not inhibited at any concentration tested (Figure 6D). Microtubules partially inhibit actin polymerization by mDia1 (Figure 6C). This partial inhibition has an IC_{50} of ~1 μM and clearly reaches a plateau (compare the 2 and 3 μM curves in Figure 6C), indicating that the partial effect is not due to subsaturating microtubule concentrations. Because these formins influence barbed-end elongation to different extents (Kovar *et al.*, 2006; Chhabra and Higgs, 2006), we quantified the inhibitory effect by determining the time required to reach polymerization of half of the actin monomers ($T_{1/2}$). By this analysis, microtubules have an IC_{50} of 47 nM for mDia2 (Figure 6D), which is similar to mDia2's K_d for microtubule binding. In contrast, microtubules inhibit mDia1 with an IC_{50} of 940 nM, significantly higher than mDia1's K_d for microtubule binding.

INF2 possesses the ability to accelerate both actin polymerization and depolymerization. For this reason, we tested the effect of microtubules on actin depolymerization by INF2-FH1FH2C, using a pyrene–actin depolymerization assay (Chhabra and Higgs, 2006). Microtubules do not inhibit actin depolymerization by INF2-FH1FH2C (Figure 6E). Of importance, none of these results (actin polymerization or depolymerization by INF2-FH1FH2C or actin polymerization by mDia1- or mDia2-FH1FH2C) is altered by the presence of 3 μM profilin (unpublished data).

Effects of actin on microtubule binding by INF2, mDia1, and mDia2

We also tested the effects of actin on microtubule binding by these formins. We used LatB-bound actin as an actin monomer pool and phalloidin-stabilized actin as an actin filament pool. In the absence of phalloidin, INF2-FH1FH2C accelerates filament depolymerization (Chhabra and Higgs, 2006), and so phalloidin is necessary to prevent accumulation of actin monomers during the experiment.

Initially, we used fluorescence microscopy assays to test the effect of actin monomers and filaments on microtubule bundling by INF2-FH1FH2C. Actin monomers strongly inhibit microtubule bundling by INF2-FH1FH2C (compare Figure 7, A and B). The presence of profilin eliminates this effect of actin monomers (Figure 7C). In contrast, actin filaments have no apparent effect on microtubule bundling by INF2-FH1FH2C (Figure 7D). We quantified these effects by counting the number of individual microtubules present in the micrographs from each condition tested. This quantification reveals that only the actin monomer treatment, and not actin filaments, results in a large increase in individual microtubules (Table 1).

INF2-FH1FH2C can bind actin filaments in two ways: it binds filament barbed ends and it binds filament sides, leading to filament severing (Chhabra and Higgs, 2006). For this reason, we conducted additional tests to favor barbed-end or side-bound INF2. To favor barbed ends, we sheared actin filaments through a 27-gauge needle immediately prior to mixing with INF2-FH1FH2C. This procedure increases barbed end concentration dramatically (Harris *et al.*, 2006). To limit the number of barbed ends, we included 10 mM potassium phosphate in the assay, which inhibits severing by INF2-FH1FH2C (Chhabra and Higgs, 2006). The presence of actin filaments does not inhibit microtubule bundling under either condition (Table 1). Our conclusion is that actin monomers, but not actin filaments, inhibit the ability of INF2-FH1FH2C to bundle microtubules.

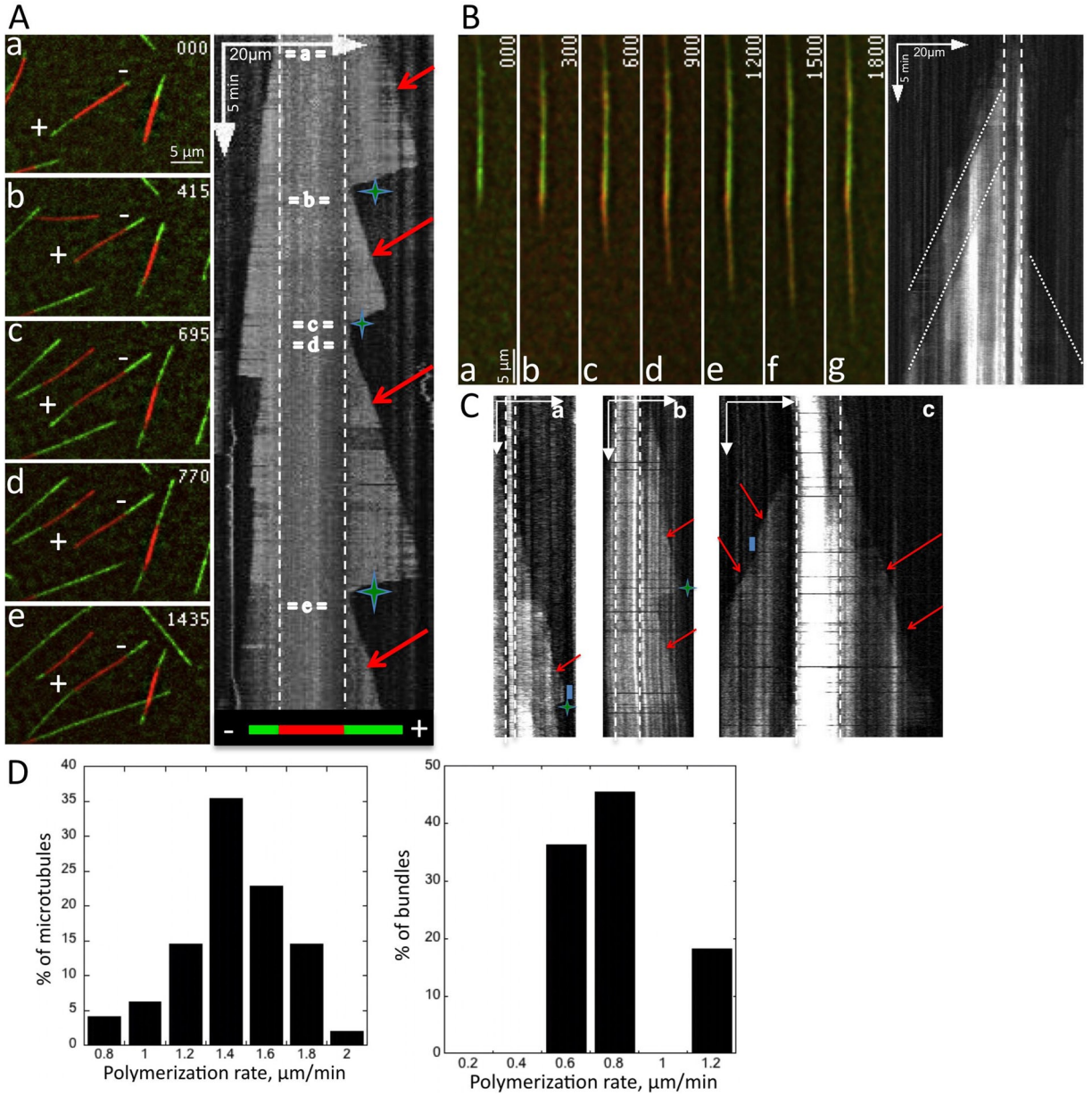

FIGURE 5: Microtubule dynamics in bundles induced by INF2-FH1FH2C. (A) Dynamic instability behavior of individual microtubules. The microtubule seeds (0.5 µM) are in red (Alexa 568–labeled tubulin), and elongating microtubule segments are in green (Alexa 488–labeled tubulin, 22 µM). (a–e) Growth and shortening at both microtubule ends observed in dual-view images from a time-lapse series (see Supplemental Movie S1). Time is in seconds; scale bar, 5 µm. The associated kymograph shows the microtubule elongation (red arrows) and catastrophe events (stars) of the microtubule at the center of the image. The microtubule seed is indicated by dotted lines. (B) Dual-view image series of the assembly of a microtubule bundle (see Supplemental Movie S2). Microtubule seed bundles were grown by adding Alexa 568–labeled tubulin (22 µM) in the presence of GFP-INF2 (0.5 µM monomer). Time is in seconds; bar, 5 µm. The corresponding kymograph indicates that the density of microtubules is high. Microtubules do not exhibit noticeable catastrophe and pause events, and microtubules grow progressively for nearly 15 min in this example. (C) Additional kymographs of microtubule bundles, showing examples of growth (red arrows), pauses (blue lines), and the only two catastrophe events observed in analyzing 11 bundles over an average of 15 min (stars). Scale bar, as in B. (D) Analysis of microtubule and bundle elongation in presence of INF2. (Left) Histogram of the mean elongation rates of microtubules during growth phases, when bundled by INF2 (n = 48). The average elongation rate is 1.54 µm/min. SD = 0.26, SE = 0.037. (Right) Histogram of the elongation rate of MT bundles (n = 11). The average elongation rate is 0.89 µm/min. SD = 0.22, SE = 0.066.

Next we used high-speed pelleting assays to examine the effect of actin on microtubule binding by INF2, mDia1, and mDia2. Because actin filaments pellet under these conditions, we could not examine the effects of filaments on microtubule binding and examined only the effect of actin monomers in these assays. The presence of actin monomers strongly inhibits microtubule binding by INF2-FH1FH2C (Figure 7E), with an IC_{50} of 0.54 µM (Figure 7F and Supplemental Figure S4A). This effect is overcome by profilin (Figure 7E).

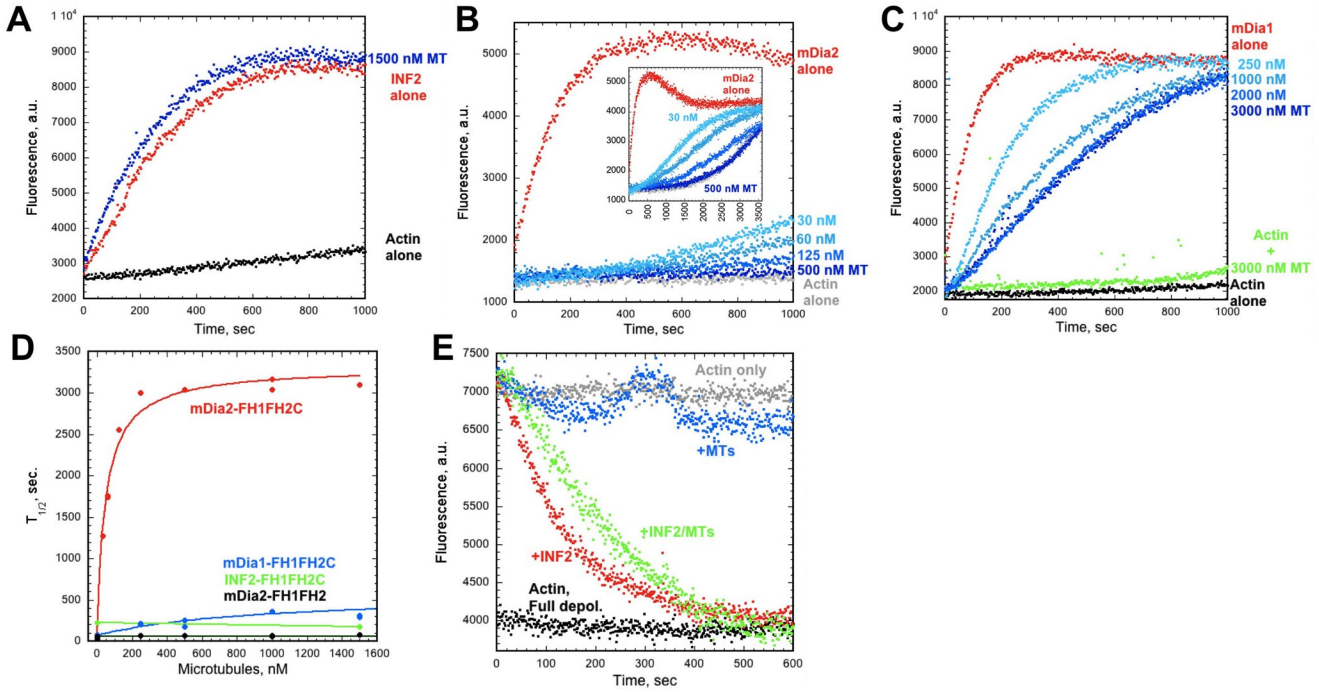

FIGURE 6: Microtubules inhibit actin polymerization by mDia1 and mDia2 but not by INF2. (A–C) Pyrene–actin polymerization assays using 1 μM actin (10% pyrene labeled) and 10 nM INF2-FH1FH2C (A), 5 nM mDia2-FH1FH2C (B), or 5 nM mDia1-FH1FH2C (C). Blue labels indicate nanomolar concentrations of MTs added in addition to the formin and actin. Inset in B shows expanded time course of polymerization (to 3600 s). (D) concentration curves of MT effects on the three formins (as well as mDia2-FH1FH2), plotted as $T_{1/2}$ (time required to reach one-half of maximal actin polymerization). $T_{1/2}$ for actin alone is 3122 s ± 152 (n = 8). (E) Pyrene–actin depolymerization assays in which 1.1 μM actin (10% pyrene labeled) is diluted to 1 μM in the presence or absence of INF2-FH1FH2C (250 nM) and/or microtubules (MTs, 750 nM). Formin monomer concentrations are given.

While testing the other formins in these pelleting assays, we experienced an interesting phenomenon, which confounded analysis somewhat. Each of these formin constructs (INF2-FH1FH2, mDia1-FH1FH2C, and mDia2-FH1FH2C) pellet to a small degree with actin monomers (Figure 7E and Supplemental Figure S4, B and C). In each case, the stoichiometry of pelleting is ~4:1 actin monomer:formin dimer, with 10% of the actin (0.25 μM) and 25% of the formin (0.125 μM formin monomer) in the pellet. This effect is inhibited by profilin for mDia2 (Figure 7E) and INF2-FH1FH2 (Supplemental Figure S4B) but not as much for mDia1 (Supplemental Figure S4C). INF2-FH1FH2C does not pellet with actin monomers in this manner.

Despite this actin monomer effect on these formins, we can still draw conclusions on their effects on microtubule binding. Similar to the INF2-FH1FH2C construct, INF2-FH1FH2 binding to microtubules is inhibited by actin monomers in a profilin-sensitive manner (Supplemental Figure S4B). In contrast, neither mDia1 nor mDia2 pelleting with microtubules is inhibited by actin monomers, either in the presence or absence of profilin (Figure 7E and Supplemental Figure S4C). In fact, actin monomer binding by the mDia2 construct actually appears to be inhibited by microtubules, since less actin monomer accumulates in the pellet when microtubules are present.

Using fluorescence microscopy, we tested directly whether these formins could interact simultaneously with phalloidin-stabilized actin filaments (labeled with Alexa 568–phalloidin) and Taxol-stabilized microtubules (labeled with Alexa 488). The actin filaments are prepolymerized in the presence of equimolar phalloidin, so that the concentration of actin monomers is extremely low in these assays and thus not likely to inhibit INF2 binding to microtubules. Mixed populations of actin filaments and microtubules do not form apparent coaggregates. In the presence of INF2-FH1FH2C, coaggregates of actin and microtubules appear, despite the fact that most of the nonaggregated actin filaments are extremely short due to INF2-mediated severing (Figure 8). INF2 does not bundle actin filaments alone (Chhabra and Higgs, 2006), suggesting that these coaggregates of actin and microtubules are due to actin filament binding by INF2 that is bound to microtubules. We cannot determine in these experiments whether the actin filaments in these aggregates are small fragments or longer filaments, but we suspect that they are INF2-severed small fragments and that INF2 is bound to their barbed ends.

mDia1-FH1FH2C does not cause extensive coaggregation (Figure 8), which is not surprising because it bundles neither actin filaments (Harris *et al.*, 2006) nor microtubules (this study). mDia2-FH1FH2C causes formation of actin filament bundles, as shown previously (Harris *et al.*, 2006). However, these bundles do not appear to associate with microtubules (Figure 8). Thus, although microtubules potently inhibit the ability of mDia2 to stimulate actin polymerization, mDia2 is still able to bundle actin filaments in the presence of microtubules.

DISCUSSION

In this study, we show that FH1FH2C constructs of INF2, mDia1, and mDia2 have distinct microtubule interaction properties (Table 2). All three formins bind microtubules with high affinity. However, the binding stoichiometries are very different, with INF2 and mDia1 dimers at ~1:3 and mDia2 dimer at close to 1:1 with tubulin dimers.

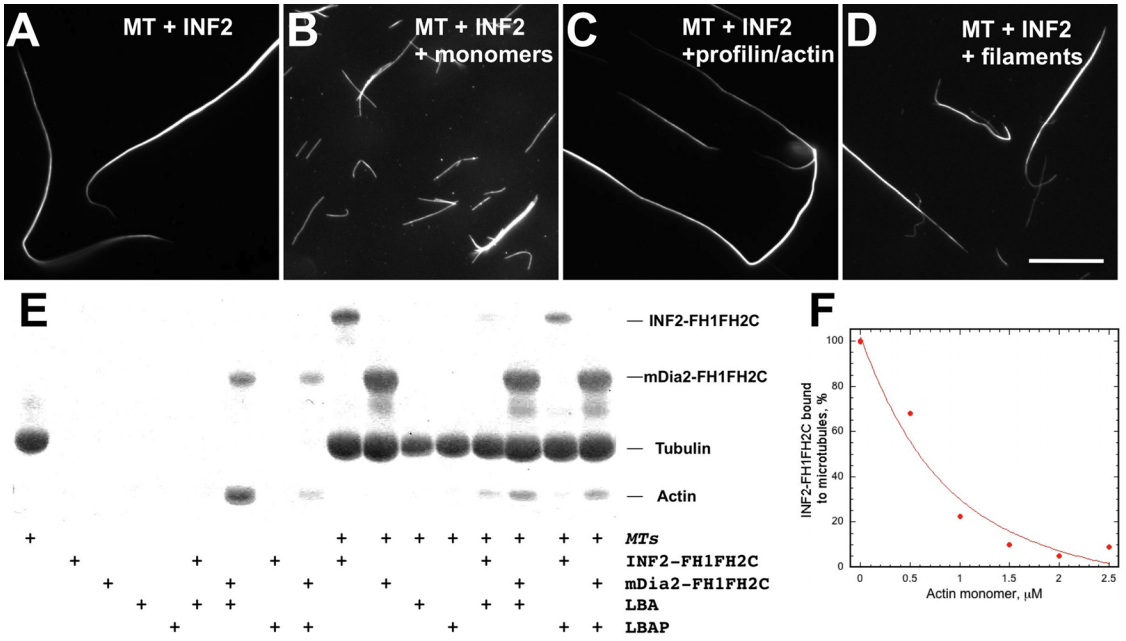

FIGURE 7: Actin monomers inhibit INF2-FH1FH2C binding to microtubules. (A–D) Fluorescence microscopy of Taxol-stabilized, Alexa 568–labeled microtubules (MT; 0.5 μM tubulin dimer) and 0.2 μM INF2-FH1FH2C alone (A), with 2 μM LatB-stabilized actin monomers (B; threefold molar excess of LatB), 2 μM profilin-bound actin monomers (C; threefold molar excess of profilin), or 2 μM phalloidin-stabilized actin filaments (D; 1.5-fold molar excess of phalloidin). Scale bar, 20 μm. Quantification of bundling is given in Table 1. (E) High-speed pelleting assays containing Taxol-stabilized microtubules (MT; 0.5 μM tubulin dimer) in the absence or presence of 0.5 μM FH1FH2C construct (INF2 or mDia2), 2.5 μM LatB-stabilized actin monomers (LBA; twofold molar excess of LatB), and 2.5 μM LatB-stabilized actin monomers with 7.5 μM profilin (LBAP). Assays are conducted in actin polymerization buffer. Pellet fractions are shown here. Formin monomer concentrations are given. (F) Concentration curve showing actin monomer inhibition of INF2-FH1FH2C binding to microtubules. INF2-FH1FH2C (monomer) and tubulin (dimer) concentrations are fixed at 0.5 μM. The *y*-axis reflects percentage of INF2-FH1FH2C bound, with 100% being the value without actin monomers present.

INF2 is a potent microtubule bundler, whereas mDia2 is a much weaker bundler and mDia1 displays no apparent microtubule bundling. Microtubules do not inhibit actin interactions by INF2, but actin monomers inhibit its microtubule–binding/bundling activities.

Condition	Number of individual microtubules
MT alone	516
MT + INF2	1
MT + INF2 + actin monomers	424
MT + INF2 + actin monomers + profilin	9
MT + INF2 + actin filaments	24
MT + INF2 + actin filaments (sheared)	13
MT + INF2 + actin filaments + PO_4	34

The number of individual microtubules present under the indicated condition was counted from fluorescence micrographs (total area counted was 143,000 μm^2 for each condition), with a larger number of free microtubules signifying lower bundling efficiency. Experimental conditions: Taxol-stabilized, Alexa 568–labeled microtubules (MT, 0.5 μM tubulin dimer), 0.2 μM INF2-FH1FH2C, 2 μM LatB-stabilized actin monomers (threefold molar excess of LatB), 2 μM profilin-bound actin monomers (threefold molar excess of profilin to LatB/actin), 2 μM phalloidin-stabilized actin filaments, 1.5-fold molar excess of phalloidin), 10 mM $NaPO_4$, pH 7.0. Shearing of actin filaments through a 27-gauge needle prior to mixing with INF2.

TABLE 1: Effect of actin monomers and actin filaments on microtubule bundling by INF2-FH1FH2C.

In contrast, mDia1 and mDia2 bind microtubules in the presence of actin monomers, but their actin polymerization activities are inhibited by microtubules. mDia2 is the most dramatic in this respect, with nanomolar microtubule concentrations causing complete inhibition of actin polymerization. INF2 causes coaggregation of microtubules with actin, whereas such coaggregation is not detectable with mDia1 or mDia2.

Differences in microtubule binding among formins

One conclusion from this study, taken with previously published work, is the following: although all formins tested can bind microtubules, the mechanisms of binding vary. An illustration of this statement is the differential contribution of the C-terminus to microtubule interactions. For INF2, the C-terminus does not contribute significant binding affinity but is necessary for microtubule bundling. For mDia2, the C-terminus is necessary for high-affinity microtubule binding, as well as to obtain 1:1 stoichiometry, since mDia2's FH1FH2 binds microtubules substoichiometrically and with only moderate affinity, in agreement with previous work (Bartolini *et al.*, 2008). In fact, the mDia2 C-terminus alone binds microtubules with significant affinity (K_d = 0.7 μM), whereas the C-termini of INF2 and mDia1 display negligible affinity.

What features of mDia2's C-terminus allow it to bind microtubules? We can narrow the important residues in this 164–amino acid region by the fact that mDia1 and mDia2 are highly homologous through the DAD, with the subsequent 109 residues of mDia2 significantly diverging from the remaining 54 residues of mDia1 (Supplemental Figure S5). Because mDia1-Cterm does not bind

	INF2	mDia2	mDia1
MT binding K_d FH1FH2C	90 nM	65 nM	60 nM
MT binding stoichiometry FH1FH2C[a]	3.4:1	0.91:1	3.09:1
MT binding K_d FH1FH2	250 nM	1800 nM	nd
MT binding stoichiometry FH1FH2[a]	2.7:1	1.7:1	nd
MT binding K_d Cterm	>20 μM	0.71 mM	>20 μM
MT binding stoichiometry Cterm[a]	—	0.6:1	—
MT bundling	Yes	Weak	No
Actin monomer effect on MT binding	Inhibits	No effect	No effect
MT effect on actin polymerization	No effect	Strong inhibition	Weak inhibition
Coaggregation of microtubules and actin	Yes	No	No
MT stabilization	Stabilizes	Stabilizes[b]	nd
Role of C-terminus	Required for bundling	Required for high-affinity/ stoichiometry binding	nd

—, too weak to measure K_d; nd, not determined.
[a]Ratio of tubulin dimer:formin dimer.
[b]From Bartolini *et al.* (2008).

TABLE 2: Properties of microtubule binding for INF2, mDia1, and mDia2.

microtubules tightly, we postulate that mDia2 binds microtubules through residues C-terminal to DAD. This region is highly basic (a pI of 10.23), which is favorable for electrostatic interactions with the acidic microtubule surface. Three basic motifs capable of binding microtubules are the K loop of the kinesin Kif1a (Okada and Hirokawa, 1999), the neck domain of the kinesin MCAK (Ovechkina *et al.*, 2002), and the MTB1 sequence at the C-terminus of INF1 (Young *et al.*, 2008). mDia2's C-terminus does not possess the salient features of these sequences (nor those of MTB2 of INF1) and thus might represent a distinct microtubule-binding motif. We do not know whether this region folds into a stable structural domain or is induced to fold upon interaction with microtubules.

The fact that mDia2-FH1FH2C binds microtubules with different stoichiometry from INF2 or mDia1 is also intriguing and appears to be a contribution of the C-terminus. We present two possible explanations for the stoichiometry differences. The first is that binding of one molecule of INF2 or mDia1 to the microtubule sterically occludes binding of neighboring molecules, resulting in a maximal occupancy of only one-third of the tubulin dimers. The microtubule-binding protein, Tau, also binds substoichiometrically to tubulin

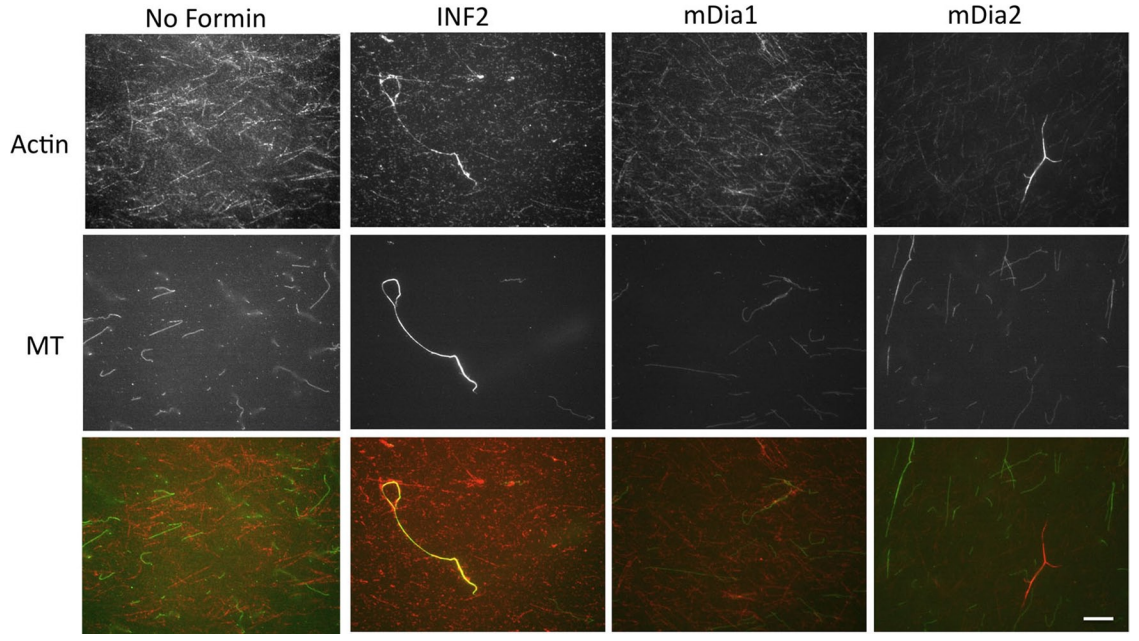

FIGURE 8: INF2 assembles coaggregates of microtubules and actin filaments. Fluorescence micrographs of Alexa 488–labeled microtubules (0.5 μM, Taxol stabilized, green) mixed with Alexa 568/phalloidin–stabilized actin filaments (1 μM, red) in the presence of 0.5 μM of the indicated FH1FH2C construct (monomer concentration) for 30 min at 23°C before imaging. Scale bar, 10 μm.

dimers, with a 1:2 ratio (Gustke *et al.*, 1994; Al-Bassam *et al.*, 2002). The second possibility is that both INF2 and mDia1 have strong preferences for microtubules containing a specific number of protofilaments. This situation occurs for doublecortin, which prefers binding to microtubules containing 13 protofilaments (Moores *et al.*, 2004). Even though 13 protofilaments is the predominant configuration in cells, it is a minority population for microtubules polymerized in vitro (Wade *et al.*, 1990; Moores *et al.*, 2004).

We do not rule out the possibility that mDia2 might dissociate into monomers in order to bind microtubules, since the mDia2 FH2 dimer has a measurable off-rate, whereas the mDia1 FH2 dimer is extremely stable (Harris *et al.*, 2006). Perhaps supporting this hypothesis, a mutation that disrupts dimerization of mDia2's FH2 still allows microtubule stabilization in cells (Bartolini *et al.*, 2008). The stability of INF2's FH2 dimer is unknown.

The potent microtubule-bundling activity of INF2 poses additional questions. Why is the C-terminus required for bundling, when the FH1-FH2 domain construct binds microtubules with reasonable affinity? We show that INF2's C-terminus alone does not bind microtubules strongly, making it very different from INF1 in this regard. One possibility is that INF2 C-terminus displays an alternate folding pattern when attached to the FH1FH2, creating a new microtubule-binding site. Another microtubule-binding protein, PRC1, is differently folded when it bridges two adjacent microtubules as opposed to when it is along the MT lattice without bundling (Subramanian *et al.*, 2010). We predict that INF2 C-terminus alone does not adopt a stably folded structure (Chhabra and Higgs, 2006). As a separate point, the fact that INF2 requires its C-terminus for bundling suggests that the FH2 can only interact with one microtubule, despite being a dimer.

Differences in actin/microtubule effects among formins

It is perhaps not surprising that formins differ in microtubule-binding mechanisms, since they differ considerably in their interactions with actin. In some respects, mDia1 is the simplest in its actin interactions, being a potent nucleator and elongation factor, but with low filament side–binding affinity and no apparent bundling activity (Li and Higgs, 2003; Harris *et al.*, 2004, 2006). In contrast, mDia2 is an actin-bundling protein, in addition to its nucleation and elongation activities (Harris *et al.*, 2006). INF2 accelerates both actin polymerization and depolymerization, the latter dependent on filament severing (Chhabra and Higgs, 2006).

The effects of microtubules on actin binding, and vice versa, vary considerably among these formins. mDia2's ability to accelerate actin polymerization is strongly inhibited by microtubules. However, mDia2 still bundles actin in the presence of microtubules, supporting previous results and suggesting that mDia2's nucleation and bundling activities are distinct (Harris *et al.*, 2006). For INF2, microtubules have no apparent effect on actin polymerization or depolymerization, whereas actin monomers inhibit microtubule binding and bundling. Nevertheless, INF2 can bind microtubules and actin filaments simultaneously. The partial inhibition by microtubules of mDia1's actin polymerization activity is curious, since microtubules bind mDia1 and mDia2 with similar affinity. These results further suggest fundamental differences in microtubule-binding mechanism, as well as the role of the C-terminus in both actin (Chhabra and Higgs, 2006; Gould *et al.*, 2011) and microtubule interactions.

It is not clear how these biochemical differences affect cellular function, but we make three points. First, actin monomer concentration is >100 μM in the cytoplasm of many mammalian cells (Pollard *et al.*, 2000), which would inhibit strongly INF2–microtubule interaction. However, high concentrations of profilin in most cells limit free actin monomer to <1 μM (Pollard *et al.*, 2000). The effect of actin monomers could depend on the activation state of the cell, since actin monomer concentration is strongly reduced upon activation (Sotiropoulos *et al.*, 1999). Second, the ability of microtubules to inhibit actin nucleation by mDia2 would depend on microtubule colocalization with active mDia2, raising potentially interesting regulatory possibilities during cytokinesis (Watanabe *et al.*, 2008, 2010) and cell motility (Gupton *et al.*, 2007). Third, formins might have differential abilities to bind microtubules simultaneously with other MAPs. Doublecortin binds at the interface of four tubulin dimers, a configuration that allows simultaneous kinesin binding (Fourniol *et al.*, 2010). Conversely, MAP2c and Tau bind along the protofilament ridge, and MAP2c at least partially occludes kinesin binding (Al-Bassam *et al.*, 2002, 2007). Myosin 1C binding to microtubules also inhibits kinesin motility (Rump *et al.*, 2011).

Our results provide fundamental information on microtubule binding but clearly are not complete pictures of formin–microtubule interactions. First, full-length formins might differ in important respects, including the following: 1) The autoinhibitory DID/DAD interaction could have important regulatory effects on microtubule binding, as it does for actin binding (Li and Higgs, 2003) and as Spire KIND does for Cappuccino/formin2 (Quinlan *et al.*, 2007); 2) the dimerization domain between the DID and the FH1 domains (Li and Higgs, 2005) might alter microtubule-binding dynamics; and 3) additional microtubule-binding sites might exist. Second, both mDia1 and mDia2 can interact with the microtubule-binding proteins EB1 and APC, requiring the FH2 domain (Wen *et al.*, 2004). Whether these interactions would enhance or inhibit the formin's affinity for microtubules is unclear, but they provide interesting possibilities for cellular function.

MATERIALS AND METHODS

Protein preparation

All formin constructs were expressed in bacteria as GST-fusion proteins, following procedures used previously (Li and Higgs, 2003, 2005; Chhabra and Higgs, 2006; Harris *et al.*, 2006). The constructs used were mDia1-FH1FH2C (mouse, amino acids 548–1255), mDia1-Cterm (1149–1255), mDia2-FH1FH2C (mouse, 521–1171), mDia2-FH1FH2 (mouse, 521–1040), mDia2-Cterm (1009–1171), INF2-FH1FH2C (human CAAX variant, 469–1249), INF2-FH1FH2 (human, 469–941), and INF2-Cterm (human CAAX variant, 941–1249). After expression, extracts were passed over glutathione–Sepharose (GE Healthcare Bio-Sciences, Piscataway, NJ), cleaved with either thrombin (mDia1, mDia2, and INF2-Cterm constructs) or tobacco etch virus protease (INF2-FH1FH2C and INF2-FH1FH2) to elute the formin construct from GST, and further purified by ion exchange chromatography on SP Sepharose (mDia1), SourceS Sepharose (mDia2 constructs), or SourceQ Sepharose (INF2 constructs). GST fusions of C-terminal constructs were eluted from glutathione–Sepharose using glutathione and then gel filtered on Superdex 200 in K50MEID (50 mM KCl, 1 mM $MgCl_2$, 1 mM ethylene glycol tetraacetic acid [EGTA], 10 mM imidazole, pH 7.0, 1 mM dithiothreitol [DTT]). All chromatographic resins were from GE Biosciences. Final buffer for formins was K50MEID.

Tubulin was prepared by polymerization–depolymerization cycling from freshly killed porcine brain. Then MAP-free tubulin was purified by two techniques, giving similar results. In France, tubulin was purified by cation exchange chromatography (EMD SO, 650 M; Merck, Darmstadt, Germany) as described (Vantard *et al.*, 1994) and then polymerization–depolymerization cycled once more and stored

as soluble dimer tubulin (concentration, ~110 μM) in BRB buffer (80 mM K-PIPES, pH 6.8, 1 mM EGTA, 1 mM DTT, and 1 mM $MgCl_2$) plus 1 mM GTP in liquid nitrogen. In the United States, tubulin was purified by anion exchange chromatography on DEAE (macro-prep DEAE; Bio-Rad, Hercules, CA) and gel filtration on Superdex 200, adapting previously described procedures (Shelanski *et al.*, 1973; Borisy *et al.*, 1974; Sloboda *et al.*, 1976; Omoto and Johnson, 1986). The Superdex 200 fraction was polymerization–depolymerization cycled once more and stored in the polymerized form (concentration, ~80 μM tubulin dimer) at −80°C after freezing in liquid nitrogen. The final buffer conditions were BRB plus 0.5 mM GTP.

Rabbit skeletal muscle actin was purified from acetone powder (Spudich and Watt, 1971) and labeled with pyrenyliodoacetamide (Cooper *et al.*, 1983). Both unlabeled and labeled actin were gel filtered on Superdex 200 (MacLean-Fletcher and Pollard, 1980) and stored in G buffer (2 mM Tris-HCl, pH 8.0, 0.5 mM DTT, 0.2 mM ATP, 0.1 mM $CaCl_2$, 0.01% sodium azide) at 4°C. Profilin (human profilin I) was expressed in bacteria and purified following published procedures (Kovar *et al.*, 2006).

Tubulin polymerization

An aliquot of frozen tubulin was removed from the −80°C freezer or from liquid nitrogen, allowed to thaw on ice, and incubated for 10 min on ice after thawing. This fraction was centrifuged at 4°C and 16,000 × *g* for 30 min in a microfuge. The protein concentration of the supernatant fraction was determined by Bradford assay (Bio-Rad), and then the fraction was diluted to 15 μM in BRB plus 2 mM GTP. This sample was incubated at 37°C for 5 min, followed by addition of the following amounts of paclitaxel (Calbiochem, La Jolla, CA) at 10-min intervals from 100-fold concentrated DMSO stocks: 0.1, 1, and 20 μM. Polymerized tubulin was kept at 23°C until used, not more than 4 h. Final conditions were 15 μM tubulin and 21.1 μM paclitaxel in BRB plus 2 mM GTP.

Pelleting assays for microtubule binding and bundling

Microtubules (0.5 μM) and formin protein were mixed in microtubule-binding buffer (MTB; K50MEID + 0.1 mM GTP, 20 μM paclitaxel, and 0.5 mM thesit [nonaethylene glycol monodecyl ether, P-9641; Sigma-Aldrich, St. Louis, MO]) at 25°C for 30 min and then centrifuged at 100,000 × *g* in a TLA100 rotor (60,000 rpm; Beckman, Coulter, Brea, CA) at 25°C for 15 min. Aliquots of supernatants were removed, and pellets were washed briefly with KMEID and resuspended in SDS–PAGE sample buffer. Proteins were resolved by SDS–PAGE, either on small (6-cm-tall Bio-Rad minigels) or large (15-cm-tall Hoeffer [Holliston, MA] gels) gels of varying density (5.75, 10, or 15% acrylamide [Bio-Rad 37.5:1 acrylamide:bis-acrylamide]), depending on the resolution required in the experiment. The α- and β-tubulin bands are resolved on the 5.75% large-format gels, resulting in a doublet, whereas they migrate as a single band on 10 or 15% gels. Gels were stained with colloidal Coomassie (Invitrogen, Carlsbad, CA) or subjected to Western blot analysis using anti-INF2 antibodies (Chhabra *et al.*, 2009). Protein in pellet was quantified by densitometry of scanned gels, using a standard curve for the protein in question generated on the same gel. Prior to the assay, all formins were diluted in MTB and centrifuged in a TLA100 at 60,000 rpm for 15 min at 25°C (supernatant used). When actin was used in these assays, it was diluted to 5 μM in the presence of 10 μM latrunculin B (LatB; Calbiochem) in MTB, incubated at 25°C for 1 h, and centrifuged in a similar manner as previously (supernatant used). When profilin was used, it was added to the LatB–actin mix at 15 μM prior to the incubation/centrifugation steps. Low-speed pelleting assays were conducted in a similar manner, except that they were centrifuged at 4000 × *g* for 10 min at 25°C and the pellets were not washed.

We note that neither affinity nor stoichiometry is significantly affected by changing buffer components from our actin polymerization buffer to a microtubule stabilization buffer (Supplemental Figure S6). We also note that the formin molar concentrations indicated in the figures use the monomer mass of each formin. However, since the FH2 domain has been shown to dimerize for all of these formins (Li and Higgs, 2005; Chhabra and Higgs, 2006), we use the dimer as the formin unit in our stoichiometry calculations.

Microscopy assays

Fluorescent tubulin (Alexa 488–labeled tubulin and Alexa 568–labeled tubulin) was prepared according to Hyman *et al.* (1991). Fluorescent tubulin (mixture of 5 μM Alexa 598–labeled tubulin and 10 μM unlabeled tubulin) was incubated at 37°C in the absence or presence of INF2 constructs and sedimented on coverslips according to Gaillard *et al.* (2008). For observations of INF2 constructs binding on Taxol-stabilized microtubules (MTs), Alexa 598–labeled MTs (0.2 μM) were incubated for 5 min with either GFP-INF2 FH1FH2C or INF2FH1FH2 (0.5 μM). Samples were observed using a fluorescence microscope (Axioplan 2 microscope [Zeiss, Thornwood, NY], 63× magnification, numerical aperture 1.3 objective, Hamamatsu [Hamamatsu, Japan] charge-coupled device Orca-1 camera, and MediaView image processing [Universal Imaging Corporation, West Chester, PA]). For negative-stain electron microscope observations, MTs (4 μM) were incubated at 20°C for 20 min with INF2 constructs (2 μM). Samples were stained with 2% (wt/vol) uranyl acetate and observed on a CM12 microscope (FEI, Eindhoven, Netherlands) operating at 120 kV.

MT dynamic behavior within INF2-FH1FH2C–induced bundles was observed using TIRF microscopy. For the assays, stable MT seeds were obtained according to Fache *et al.* (2010). Seed bundles were obtained by incubating 1 μM MT seeds with 1 μM INF2FH1FH2C for 10 min at room temperature. To keep MT seeds within the excitation field, we used NeutrAvidin Biotin-Binding Protein (Pierce, Thermo Fisher Scientific, Rockford, IL) specific to biotin to adhere MT seeds to the cover glass surface according to Fache *et al.* (2010). Seeds and MT seed bundles were then elongated by the addition of 22 μM tubulin (17 μM unlabeled tubulin, 5 μM of Alexa-labeled tubulin), in the absence or the presence of 1 μM INF2FH1FH2C, 1 mM GTP, an oxygen scavenger cocktail (2 mg/ml glucose, 80 μg/ml catalase, 0.67 mg/ml glucose oxidase), and 1.5% bovine serum albumin. Experiments were conducted in a final volume of 5 μl between glass covered with poly(L-lysine)–poly(ethylene glycol) in order to limit interactions between MTs and the coverglass. MT dynamics was visualized at 32°C using an objective-based total internal fluorescence microscope (Nikon TE2000-E). Excitation was achieved using 491- and a 561-nm lasers to visualize GFP and Alexa 568, respectively. Time-lapse microscopy (one frame every 2 or 5 s) was performed for 30 min using MetaMorph software, version 6.3r7 (Molecular Devices, Sunnyvale, CA), and frames were analyzed using MetaMorph; "equalize light," "basic filter," and "flatten background" were the filters used to improve the signal/noise ratio. MT bundle elongation and dynamics were analyzed using kymographs generated by MetaMorph and analyzed with ImageJ (Bethesda, MD).

Actin polymerization and depolymerization assays

All assays were performed on a mixture of 90% unlabeled/10% pyrene-labeled actin, using an Infinity M-1000 fluorescence plate

reader (Tecan, Männedorf, Switzerland) or a PC1 spectrofluorimeter (ISS, Champaign, IL). For polymerization assays, 3.33 μM actin monomers in G buffer were converted to the Mg^{2+} salt by addition of 0.1 volume of 10 mM EGTA/1 mM $MgCl_2$ for 2 min at 23°C before starting the assay. Formins and microtubules were premixed at 23°C in buffer containing 75 mM KCl, 1.7 mM $MgCl_2$, 1.7 mM EGTA, 15 mM imidazole-HCl, pH 7.0, 16 mM K-PIPES, pH 6.9, 0.1 mM GTP, 0.5 mM thesit, 0.75 mM DTT, and 9 μM paclitaxel. Assays were started by mixing 1 volume of actin with 2 volumes of formin–microtubule mix and monitored for pyrene fluorescence at 365-nm excitation and 407-nm emission at 27°C.

For depolymerization assays, 1.1 μM actin was polymerized at least 15 h at 23°C in K50MEID + 0.5 mM thesit, then mixed with 0.1 volume of formin–microtubule mix in K50MEID + 0.5 mM thesit, 40 mM K-PIPES, pH 6.9, 0.5 mM $MgCl_2$, 0.5 mM EGTA, 0.25 mM GTP, and 10 μM paclitaxel. Decrease in pyrene fluorescence was monitored as previously noted. In the depolymerization assays, ATP concentration was <4 μM (contribution from the actin stocks).

ACKNOWLEDGMENTS

We thank Chuck Wooster and Norah Lake at Sunrise Farm (Hartford, VT) for supplying the porcine raw material for tubulin preparation. We also thank Margot Quinlan for comments on the manuscript and Curt Lemobius for his dynamic energy. This work was supported by National Institutes of Health Grants RO1 GM069818 and DK088826 to H.N.H. and by Centre Nationale de la Recherche Scientifique and Commissariat à l'Energie Atomique et aux Energies Alternatives for J.G., E.N., L.B., and M.V.

REFERENCES

Al-Bassam J, Ozer RS, Safer D, Halpain S, Milligan RA (2002). MAP2 and tau bind longitudinally along the outer ridges of microtubule protofilaments. J Cell Biol 157, 1187–1196.

Al-Bassam J, Roger B, Halpain S, Milligan RA (2007). Analysis of the weak interactions of ADP-Unc104 and ADP-kinesin with microtubules and their inhibition by MAP2c. Cell Motil Cytoskeleton 64, 377–389.

Azoury J, Lee KW, Georget V, Rassinier P, Leader B, Verlhac MH (2008). Spindle positioning in mouse oocytes relies on a dynamic meshwork of actin filaments. Curr Biol 18, 1514–1519.

Bartolini F, Gundersen GG (2010). Formins and microtubules. Biochim Biophys Acta 1803, 164–173.

Bartolini F, Moseley JB, Schmoranzer J, Cassimeris L, Goode BL, Gundersen GG (2008). The formin mDia2 stabilizes microtubules independently of its actin nucleation activity. J Cell Biol 181, 523–536.

Borisy GG, Olmsted JB, Marcum JM, Allen C (1974). Microtubule assembly in vitro. Fed Proc 33, 167–174.

Cheng L, Zhang J, Ahmad S, Rozier L, Yu H, Deng H, Mao Y (2011). Aurora B regulates formin mDia3 in achieving metaphase chromosome alignment. Dev Cell 20, 342–352.

Chhabra ES, Higgs HN (2006). INF2 is a WH2 motif-containing formin that severs actin filaments and accelerates both polymerization and depolymerization. J Biol Chem 281, 26754–26767.

Chhabra ES, Ramabhadran V, Gerber SA, Higgs HN (2009). INF2 is an endoplasmic reticulum-associated formin protein. J Cell Sci 122, 1430–1440.

Cooper JA, Walker SB, Pollard TD (1983). Pyrene actin: documentation of the validity of a sensitive assay for actin polymerization. J Muscle Res Cell Motil 4, 253–262.

Dahlgaard K, Raposo AA, Niccoli T, St Johnston D (2007). Capu and Spire assemble a cytoplasmic actin mesh that maintains microtubule organization in the *Drosophila* oocyte. Dev Cell 13, 539–553.

Eisenmann KM, West RA, Hildebrand D, Kitchen SM, Peng J, Sigler R, Zhang J, Siminovitch KA, Alberts AS (2007). T cell responses in mammalian diaphanous-related formin mDia1 knock-out mice. J Biol Chem 282, 25152–25158.

Fache V, Gaillard J, Van Damme D, Geelen D, Neumann E, Stoppin-Mellet V, Vantard M (2010). *Arabidopsis* kinetochore fiber-associated MAP65–4 cross-links microtubules and promotes microtubule bundle elongation. Plant Cell 22, 3804–3815.

Fourniol FJ, Sindelar CV, Amigues B, Clare DK, Thomas G, Perderiset M, Francis F, Houdusse A, Moores CA (2010). Template-free 13-protofilament microtubule-MAP assembly visualized at 8 A resolution. J Cell Biol 191, 463–470.

Gaillard J, Neumann E, Van Damme D, Stoppin-Mellet V, Ebel C, Barbier E, Geelen D, Vantard M (2008). Two microtubule-associated proteins of *Arabidopsis* MAP65s promote antiparallel microtubule bundling. Mol Biol Cell 19, 4534–4544.

Gasteier JE, Schroeder S, Muranyi W, Madrid R, Benichou S, Fackler OT (2005). FHOD1 coordinates actin filament and microtubule alignment to mediate cell elongation. Exp Cell Res 306, 192–202.

Gomez TS, Kumar K, Medeiros RB, Shimizu Y, Leibson PJ, Billadeau DD (2007). Formins regulate the actin-related protein 2/3 complex-independent polarization of the centrosome to the immunological synapse. Immunity 26, 177–190.

Goode BL, Drubin DG, Barnes G (2000). Functional cooperation between the microtubule and actin cytoskeletons. Curr Opin Cell Biol 12, 63–71.

Gould CJ, Maiti S, Michelot A, Graziano BR, Blanchoin L, Goode BL (2011). The formin DAD domain plays dual roles in autoinhibition and actin nucleation. Curr Biol 21, 384–390.

Gupton SL, Eisenmann K, Alberts AS, Waterman-Storer CM (2007). mDia2 regulates actin and focal adhesion dynamics and organization in the lamella for efficient epithelial cell migration. J Cell Sci 120, 3475–3487.

Gustke N, Trinczek B, Biernat J, Mandelkow EM, Mandelkow E (1994). Domains of tau protein and interactions with microtubules. Biochemistry 33, 9511–9522.

Harris ES, Gauvin TJ, Heimsath EG, Higgs HN (2010). Assembly of filopodia by the formin FRL2 (FMNL3). Cytoskeleton 67, 755–772.

Harris ES, Li F, Higgs HN (2004). The mouse formin, FRLa, slows actin filament barbed end elongation, competes with capping protein, accelerates polymerization from monomers, and severs filaments. J Biol Chem 279, 20076–20087.

Harris ES, Rouiller I, Hanein D, Higgs HN (2006). Mechanistic differences in actin bundling activity of two mammalian formins, FRL1 and mDia2. J Biol Chem 281, 14383–14392.

Higgs HN (2005). Formin proteins: a domain-based approach. Trends Biochem Sci 30, 342–353.

Higgs HN, Peterson KJ (2005). Phylogenetic analysis of the formin homology 2 (FH2) domain. Mol Biol Cell 16, 1–13.

Hyman A, Drechsel D, Kellogg D, Salser S, Sawin K, Steffen P, Wordeman L, Mitchison T (1991). Preparation of modified tubulins. Methods Enzymol 196, 478–485.

Ishizaki T, Morishima Y, Okamoto M, Furuyashiki T, Kato T, Narumiya S (2001). Coordination of microtubules and the actin cytoskeleton by the Rho effector mDia1. Nat Cell Biol 3, 8–14.

Korobova F, Svitkina T (2010). Molecular architecture of synaptic actin cytoskeleton in hippocampal neurons reveals a mechanism of dendritic spine morphogenesis. Mol Biol Cell 21, 165–176.

Kovar DR, Harris ES, Mahaffy R, Higgs HN, Pollard TD (2006). Control of the assembly of ATP- and ADP-actin by formins and profilin. Cell 124, 423–435.

Li F, Higgs HN (2003). The mouse formin mDia1 is a potent actin nucleation factor regulated by autoinhibition. Curr Biol 13, 1335–1340.

Li F, Higgs HN (2005). Dissecting requirements for auto-inhibition of actin nucleation by the formin, mDia1. J Biol Chem 280, 6986–6992.

Li H, Guo F, Rubinstein B, Li R (2008). Actin-driven chromosomal motility leads to symmetry breaking in mammalian meiotic oocytes. Nat Cell Biol 10, 1301–1308.

MacLean-Fletcher S, Pollard TD (1980). Mechanisms of action of cytochalasin B on actin. Cell 20, 329–341.

McTigue MA, Williams DR, Tainer JA (1995). Crystal structure of a schistosomal drug and vaccine target: glutathione *S*-transferase from *Schistosoma japonica* and its complex with the leading antischistosomal drug praziquantel. J Mol Biol 246, 121–27.

Moores CA, Perderiset M, Francis F, Chelly J, Houdusse A, Milligan RA (2004). Mechanism of microtubule stabilization by doublecortin. Mol Cell 14, 833–839.

Moseley JB, Goode BL (2005). Differential activities and regulation of *Saccharomyces cerevisiae* formin proteins Bni1 and Bnr1 by Bud6. J Biol Chem 280, 28023–28033.

Okada K, Bartolini F, Deaconescu AM, Moseley JB, Dogic Z, Grigorieff N, Gundersen GG, Goode BL (2010). Adenomatous polyposis coli protein nucleates actin assembly and synergizes with the formin mDia1. J Cell Biol 189, 1087–1096.

Okada Y, Hirokawa N (1999). A processive single-headed motor: kinesin superfamily protein KIF1A. Science 283, 1152–1157.
Omoto CK, Johnson KA (1986). Activation of the dynein adenosinetriphosphatase by microtubules. Biochemistry 25, 419–427.
Ovechkina Y, Wagenbach M, Wordeman L (2002). K-loop insertion restores microtubule depolymerizing activity of a "neckless" MCAK mutant. J Cell Biol 159, 557–562.
Paul AS, Pollard TD (2009). Review of the mechanism of processive actin filament elongation by formins. Cell Motil Cytoskeleton 66, 606–617.
Pollard TD, Blanchoin L, Mullins RD (2000). Molecular mechanisms controlling actin filament dynamics in nonmuscle cells. Annu Rev Biophys Biomol Struct 29, 545–576.
Quinlan ME, Hilgert S, Bedrossian A, Mullins RD, Kerkhoff E (2007). Regulatory interactions between two actin nucleators, Spire and Cappuccino. J Cell Biol 179, 117–128.
Rodriguez OC, Schaefer AW, Mandato CA, Forscher P, Bement WM, Waterman-Storer CM (2003). Conserved microtubule-actin interactions in cell movement and morphogenesis. Nat Cell Biol 5, 599–609.
Rosales-Nieves AE, Johndrow JE, Keller LC, Magie CR, Pinto-Santini DM, Parkhurst SM (2006). Coordination of microtubule and microfilament dynamics by *Drosophila* Rho1, Spire and Cappuccino. Nat Cell Biol 8, 367–376.
Rottner K, Hanisch J, Campellone KG (2010). WASH, WHAMM and JMY: regulation of Arp2/3 complex and beyond. Trends Cell Biol 20, 650–661.
Rump A, Scholz T, Thiel C, Hartmann FK, Uta P, Hinrichs MH, Taft MH, Tsiavaliaris G (2011). Myosin-1C associates with microtubules and stabilizes the mitotic spindle during cell division. J Cell Sci 124, 2521–2528.
Schliwa M, van Blerkom J (1981). Structural interaction of cytoskeletal components. J Cell Biol 90, 222–235.
Schuh M, Ellenberg J (2008). A new model for asymmetric spindle positioning in mouse oocytes. Curr Biol 18, 1986–1992.
Shelanski ML, Gaskin F, Cantor CR (1973). Microtubule assembly in the absence of added nucleotides. Proc Natl Acad Sci USA 70, 765–768.
Sloboda RD, Dentler WL, Rosenbaum JL (1976). Microtubule-associated proteins and the stimulation of tubulin assembly in vitro. Biochemistry 15, 4497–4505.
Sotiropoulos A, Gineitis D, Copeland J, Treisman R (1999). Signal-regulated activation of serum response factor is mediated by changes in actin dynamics. Cell 98, 159–169.
Spudich JA, Watt S (1971). The regulation of rabbit skeletal muscle contraction. I. Biochemical studies of the interaction of the tropomyosin-troponin complex with actin and the proteolytic fragments of myosin. J Biol Chem 246, 4866–4871.
Subramanian R, Wilson-Kubalek EM, Arthur CP, Bick MJ, Campbell EA, Darst SA, Milligan RA, Kapoor TM (2010). Insights into antiparallel microtubule crosslinking by PRC1, a conserved nonmotor microtubule binding protein. Cell 142, 433–443.
Theurkauf WE (1994). Premature microtubule-dependent cytoplasmic streaming in cappuccino and spire mutant oocytes. Science 265, 2093–2096.
Tsukada M, Proksch A, Ungewickell E, Eichele G (2005). Doublecortin association with actin filaments is regulated by neurabin II. J Biol Chem 280, 11361–11368.
Vaillant DC, Copeland SJ, Davis C, Thurston SF, Abdennur N, Copeland JW (2008). Interaction of the N- and C-terminal autoregulatory domains of FRL2 does not inhibit FRL2 activity. J Biol Chem 283, 33750–33762.
Vantard M, Peter C, Fellous A, Schellenbaum P, Lambert AM (1994). Characterization of a 100-kDa heat-stable microtubule-associated protein from higher plants. Eur J Biochem 220, 847–853.
Wade RH, Chretien D, Job D (1990). Characterization of microtubule protofilament numbers. How does the surface lattice accommodate? J Mol Biol 212, 775–786.
Watanabe S, Ando Y, Yasuda S, Hosoya H, Watanabe N, Ishizaki T, Narumiya S (2008). mDia2 induces the actin scaffold for the contractile ring and stabilizes its position during cytokinesis in NIH 3T3 cells. Mol Biol Cell 19, 2328–2338.
Watanabe S, Okawa K, Miki T, Sakamoto S, Morinaga T, Segawa K, Arakawa T, Kinoshita M, Ishizaki T, Narumiya S (2010). Rho and anillin-dependent control of mDia2 localization and function in cytokinesis. Mol Biol Cell 21, 3193–3204.
Waterman-Storer C, Duey DY, Weber KL, Keech J, Cheney RE, Salmon ED, Bement WM (2000). Microtubules remodel actomyosin networks in *Xenopus* egg extracts via two mechanisms of F-actin transport. J Cell Biol 150, 361–376.
Wen Y, Eng CH, Schmoranzer J, Cabrera-Poch N, Morris EJS, Chen M, Wallar BJ, Alberts AS, Gundersen GG (2004). EB1 and APC bind to mDia to stabilize microtubules downstream of Rho and promote cell migration. Nat Cell Biol 6, 820–830.
Xu Y, Moseley JB, Sagot I, Poy F, Pellman D, Goode BL, Eck MJ (2005). Crystal structures of a Formin Homology-2 domain reveal a tethered dimer architecture. Cell 116, 711–723.
Yasuda S, Oceguera-Yanez F, Kato T, Okamoto M, Yonemura S, Terada Y, Ishizaki T, Narumiya S (2004). Cdc42 and mDia3 regulate microtubule attachment to kinetochores. Nature 428, 767–771.
Young KG, Thurston SF, Copeland S, Smallwood C, Copeland JW (2008). Inf1 is a novel microtubule-associated formin. Mol Biol Cell 19, 5168–5180.
Zhou F, Leder P, Martin SS (2006). Formin-1 protein associates with microtubules through a peptide domain encoded by exon-2. Exp Cell Res 312, 1119–1126.